

Boltzmann Sampling by Diabatic Quantum Annealing

Ju-Yeon Gyhm,^{1,*} Gilhan Kim,^{1,*} Hyukjoon Kwon,² and Yongjoo Baek^{1,†}

¹*Department of Physics and Astronomy & Center for Theoretical Physics, Seoul National University, Seoul 08826, Korea*

²*School of Computational Sciences, Korea Institute for Advanced Study, Seoul 02455, Korea*

(Dated: March 21, 2025)

It has been proposed that diabatic quantum annealing (DQA), which turns off the transverse field at a finite speed, produces samples well described by the Boltzmann distribution. We analytically show that, up to linear order in quenching time, the DQA approximates a high-temperature Boltzmann distribution. Our theory yields an explicit relation between the quenching rate of the DQA and the temperature of the Boltzmann distribution. Based on this result, we discuss how the DQA can be utilized to train the Restricted Boltzmann Machine (RBM).

I. INTRODUCTION

Based on the adiabatic theorem [6], quantum annealing [7] has been proposed as a method to achieve optimization via quantum fluctuations rather than thermal fluctuations. Remarkably, recent studies [5, 8, 9] have reported that the samples produced by the D-wave quantum annealers [10] are close to the Boltzmann distribution, although theoretical justifications are lacking. On the other hand, the effect of quantum machine's physical temperature is also studied. D-wave's official document [11] compares the Boltzmann sampling performance between their quantum annealer and classical algorithms, the temperature (12.8 mK) here is the machine's physical temperature which we cannot control.

We note that finding the ground state via conventional quantum annealing can be viewed as sampling the Boltzmann distribution at zero temperature ($\beta = \infty$). On the other hand, if the transverse external field is instantaneously quenched to zero, the resulting samples should obey the infinite-temperature Boltzmann distribution ($\beta = 0$). Then, one can naturally conjecture that diabatic quantum annealing (DQA), which turns off the transverse field at a finite speed, would lead to the Boltzmann distribution at a finite temperature.

In this study, we analytically show that the projective probabilities of states obtained through a finite-speed linear decrease in the transverse field approximately corresponds to the Boltzmann sampling at a finite temperature. And it should be noted that when sampling using this new methodology, all samples are independent without having to consider decorrelation time. This point will be discussed in a bit more at Sec. IV.

We test our prediction using the two-dimensional and the all-to-all Ising models, observing an agreement between the two distributions. While this agreement is limited to the high-temperature regime, it is good enough to be used in the training of restricted Boltzmann machines (RBMs) whose weights remain small throughout the training.

The rest of the paper is organized as follows. In Sec. II, we describe our theory that matches annealing speed to temperature. In Sec. III, we check how well our proposed method reproduces the statistics of the system's physical observables. In Sec. IV, we compare the target Boltzmann distribution of the RBMs with the estimated distribution obtained by our method. In Sec. V, we show the details of our analytical derivation. Finally, we summarize our findings and conclude in Sec. VI.

II. DIABATIC QUATNUM ANNEALING

We consider the conventional quantum annealing model using the x -directional magnetic field and the problem Hamiltonian, whose eigenbasis are z -directional spin configuration states. The time-dependent Hamiltonian for quantum annealing is given by

$$\hat{H}(t) = A(t)\hat{H}_x + B(t)\hat{H}_{\text{sg}}, \quad (1)$$

for time, $0 \leq t \leq T$. $A(t)$ and $B(t)$ are arbitrary functions that determine a time dependency of the Hamiltonian. They have the boundary conditions, $A(0) \gg B(0)$ at the initial time, and $A(T) \ll B(T)$ at the final time to ensure problem-solving.

$\hat{H}_x = \sum_{i=1}^N \sigma_i^x$ is the Hamiltonian of the x -directional magnetic field, while \hat{H}_{sg} is arbitrary spin glass Hamiltonian generally described by

$$\hat{H}_{\text{sg}} = \sum_{1 \leq i \leq N} h_i \sigma_i^z + \sum_{1 \leq i < j \leq N} J_{ij} \sigma_i^z \sigma_j^z \quad (2)$$

The final state, $|\psi_f\rangle$, at the end of quantum annealing with given $A(t)$ and $B(t)$, is described by unitary evolution as

$$|\psi_f\rangle = \mathcal{T} \int_0^T dt \exp(-i\hat{H}(t)) \bigotimes_{i=1}^N |X-\rangle_i. \quad (3)$$

We assume that the state is initially prepared to the ground state of \hat{H}_x , as $|\psi_i\rangle = \bigotimes_{i=1}^N |X-\rangle_i$ at $t = 0$, where $|X-\rangle_i$ is an eigenstate of σ_i^x as $\sigma_i^x |X-\rangle_i = -|X-\rangle$. We use the atomic units in this letter as $\hbar = 1$. The projective probabilities of $|\psi_f\rangle$ by spin- z configurations, \mathbf{s} are magnitude of overlaps $P_{\text{proj}}(\mathbf{s}) = |\langle \mathbf{s} | \psi_f \rangle|^2$.

* These authors contributed equally to this work.

† y.baek@snu.ac.kr

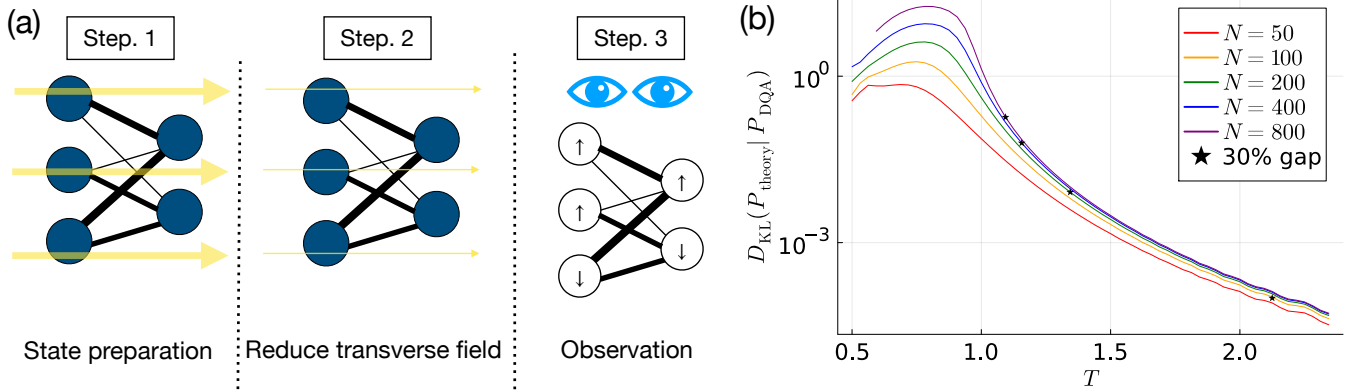


FIG. 1. (a) Sampling scheme by DQA. First, encode interactions, bias vectors and transverse field to the spin system. Second, reduce the transverse field as scheduled. Third, observe the spins and save the configuration. By repeating the step 1-3 multiple times, sample set can be constructed. (b) The Kullback-Leibler divergence between the theoretical Boltzmann distribution of all-to-all Ising model P_{theory} and their corresponding DQA-estimated distribution P_{DQA} . The star-shape marks denote the points where the gap between Kullback-Leibler divergence between two nearest lines are 1 : 1.3. As the system size increases, the star moves closer to T_C , indicating that the error rate of DQA is negligible for large N limit, hence, sampling performance of DQA is reliable in disordered phase.

Conventional quantum annealing uses the adiabatic region, where $A(t)$ and $B(t)$ slowly vary with respect to the energy gap between the ground state and the first excited state of $\hat{H}(t)$ for any instant time, t . At the region, the state, $|\psi(t)\rangle$, is the ground state of $\hat{H}(t)$. Using the property, conventional quantum annealing is considered the efficient way to obtain the ground state of \hat{H}_{sg} . Meanwhile, we consider the quantum annealing process as the Boltzmann sampler at the out of the adiabatic region.

The intuitive motivation comes from extreme cases; the adiabatic region and the quenching region. At the adiabatic region, the $|\psi\rangle$ is effectively the ground state of \hat{H}_{sg} , whose $P_{\text{proj}}(\mathbf{s})$ can be regarded as the Boltzmann distribution of \hat{H}_{sg} with zero temperature. Likewise, we can regard $|\psi_f\rangle$ as the Boltzmann distribution with infinity temperature, since the final state is almost equal to the initial state as $|\psi_f\rangle \approx |\psi_i\rangle = \bigotimes_{i=1}^N |X-\rangle_i$, whose $P_{\text{proj}}(\mathbf{s})$ are $1/2^N$ for any spin configuration \mathbf{s} . At two extreme regions, P_{proj} are the same as the Boltzmann distribution with two extreme temperatures, which yields the question about whether $P_{\text{QA}}((\mathbf{s}))$ can represent the Boltzmann distribution with the finite temperature, $\beta = 1$.

We prove there is a relationship between the projective and the Boltzmann distribution,

Theorem 1. The projective probability, $P_{\text{proj}}(\mathbf{s})$, is driven by modified Hamiltonian,

$$\hat{H}'_{\text{sg}} = \sum_{1 \leq i \leq N} h_i \sigma_i^z + c_2 \sum_{1 \leq i < j \leq N} J_{ij} \sigma_i^z \sigma_j^z, \quad (4)$$

with modified parameter, c_2 . $P_{\text{proj}}(\mathbf{s})$ is approximately equal to the Boltzmann distribution, with $\beta = 1$ and the

original Hamiltonian,

$$\hat{H}_{\text{sg}} = \sum_{1 \leq i \leq N} h_i \sigma_i^z + \sum_{1 \leq i < j \leq N} J_{ij} \sigma_i^z \sigma_j^z, \quad (5)$$

as $P_B(\mathbf{s}) = \frac{1}{Z} \langle \mathbf{s} | \exp(-H_{\text{sg}}) | \mathbf{s} \rangle$, if the following conditions hold;

$$1 = 2 \int_0^T dt B(t) \sin \left(2 \int_t^T ds A(s) \right), \quad (6)$$

and

$$c_2 = \frac{\int_0^T dt B(t) \sin \left(2 \int_t^T ds A(s) \right)}{\int_0^T dt B(t) \sin \left(4 \int_t^T ds A(s) \right)}, \quad (7)$$

The proof is using the Dyson series. Using the Dyson series, we construct the perturbative series of $P_{\text{proj}}(\mathbf{s})$ by h_i and J_{ij} . After gaining the series, we compare it with a series of Boltzmann distribution. For detailed calculation, we refer readers to the Appendix.

Formally, the Boltzmann distribution is given as $P_B(\mathbf{r}) = \frac{1}{Z} e^{-\beta E'_{\mathbf{r}}}$, where $E'_{\mathbf{r}} = \langle \mathbf{r} | \hat{H}'_{\text{P}} | \mathbf{r} \rangle$ and Z is the partition function, $Z = \sum_{\mathbf{r}} e^{-\beta E'_{\mathbf{r}}}$. β and c_2 are not fitting parameters but are uniquely determined by the lowest order of the Dyson series. Since the relationship is valid for the lowest order of energy, the relationship is only valid for the high temperature limit. We refer to the chapter V for detailed proof and how $A(t)$ and $B(t)$ determine β and c_2 .

Although the relationship exists for any $A(t)$ and $B(t)$, we mainly deal with one of the simplest schedules, $A(t) = \alpha(T - t)$ and $B(t) = 1$. The above linear function $A(t)$ and $B(t)$ determine the temperature as

$$\beta = \sqrt{\frac{\pi}{2\alpha}} \quad (8)$$

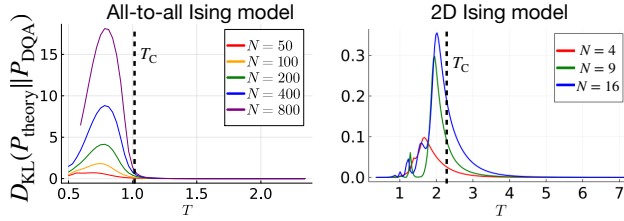


FIG. 2. Kullback-Leibler divergence between target distribution and its DQA-estimated distributions (left: all to all Ising model, right: 2D Ising model). For high temperature distributions, the DQA's estimation performance is appreciable. However, near critical temperature and low temperature, it is not.

and modifying factor as $c_2 = 1/\sqrt{2}$.

III. COMPARISON BETWEEN THE ESTIMATED DISTRIBUTION AND THE BOLTZMANN DISTRIBUTION

We calculate the Kullback–Leibler divergence for several well-known models to confirm how the estimated distribution is similar to the Boltzmann distribution. The Kullback–Leibler divergence represents how one distribution is different from the true distribution, which is written by

$$D_{KL}(P_B \| P_Q) = \sum_{\mathbf{r}} P_B(\mathbf{r}) \ln \frac{P_B(\mathbf{r})}{P_Q(\mathbf{r})}. \quad (9)$$

We simulate the quantum annealing with problem Hamiltonians as representative models composed of the two-dimensional Ising model and all-to-all Ising model. The Hamiltonian of all-to-all Ising model is written as

$$\hat{H}_P = - \sum_{i < j} \frac{1}{N} \sigma_i^z \sigma_j^z \quad (10)$$

which has a critical point at $\beta_C = 1$. Since the all-to-all Ising model satisfies the mean-field theory, we introduce the two-dimensional Ising model which does not follow the mean-field theory to confirm whether the mean-field theory is significant for the quality of estimated distribution. The Hamiltonian of the two-dimensional Ising model is given by

$$\hat{H}_P = - \sum_{1 \leq i, j \leq L} (\sigma_{i,j}^z \sigma_{i+1,j}^z + \sigma_{i,j}^z \sigma_{i,j+1}^z), \quad (11)$$

for L length square lattice with periodic condition. The critical point is known as $\beta_C = 2/\ln(1 + \sqrt{2})$

By numerical calculation of time ordered integral, Eq. (3), we prepare the estimated probability, P_Q , with different time gradient, α , which have corresponding Boltzmann distribution, P_B , with different $\beta = \sqrt{\pi}/2\alpha$. Fig. 2 provides the dependence of Kullback–Leibler divergence on β . They describes the Kullback–Leibler divergence between the target Boltzmann distribution and

the estimated distribution. For paramagnetic phases, the Kullback–Leibler divergences are very close to zero, while it is very high near critical point and low temperature regimes.

Fig. 2 shows the Kullback–Leibler divergences between the theoretical Boltzmann distributions and the estimated distribution using the DQA. Both the all-to-all Ising model and the 2D Ising model's cases, the DQA is appreciable for high temperature regime, while near critical temperature and low temperature regime, it is not. Also, as the system sizes increases, the temperature that the DQA's quality decrease increases.

The quantum expectation value for an observable, \hat{O} , is given as $\overline{O}_Q = \langle \psi_f | \hat{O} | \psi_f \rangle$. When the observable has the basis as $|\mathbf{r}\rangle$, the quantum expectation value becomes, $\overline{O}_Q = \sum_{\mathbf{r}} P_Q(\mathbf{r}) \langle \mathbf{r} | \hat{O} | \mathbf{r} \rangle$. The corresponding Boltzmann distribution has the thermal expectation given by $\overline{O}_B = \sum_{\mathbf{r}} P_B(\mathbf{r}) \langle \mathbf{r} | \hat{O} | \mathbf{r} \rangle$ for observable \hat{O} . Obviously, the deviation of the quantum expectation from the thermal expectation indicates how both distributions differ.

Fig. 3 shows the behaviors of the observables–magnetization, magnetic susceptibility and the binder cumulant. For both models, the differences between theoretical values and the estimated values using the DQA are maximum near critical temperature. Unlike the Fig. 2, the estimated values are very close to theoretical values at low temperature. This phenomenon is because at low temperatures, there is no state other than the ground state.

IV. ESTIMATED DISTRIBUTION OF THE RESTRICTED BOLTZMANN MACHINE

The goal of restricted Boltzmann machines (RBMs) training is to decrease the Kullback–Leibler divergence between the training data's distribution and the model's distribution. Exact estimation of the model's distribution is limited because of the large degree of freedom. Hence, the efficient sampling method is suggested for RBMs training as contrastive divergence algorithm, persistent contrastive divergence algorithm [12] and parallel tempering [13, 14], which are based on Markov chain Monte Carlo simulation. Our approach, DQA, deviates from Monte Carlo simulation by using a quantum machine.

In the case of the Markov chain Monte Carlo algorithms, there must be an appropriate decorrelation time $\tau \sim (\text{system size})^z$ between the points where sampling is performed, z stands for the dynamical critical exponent. Hence, as the system size increases, and as the RBMs are near critical regime, the number of decorrelation steps we need to have increases rapidly. In practical level, this point is rarely taken into consideration, and sampling is simply performed with appropriate intervals, such as 3 steps or 5 steps, as a rule of thumb. Since all samples obtained using DQA are completely independent to each other, there is no need to consider this point.

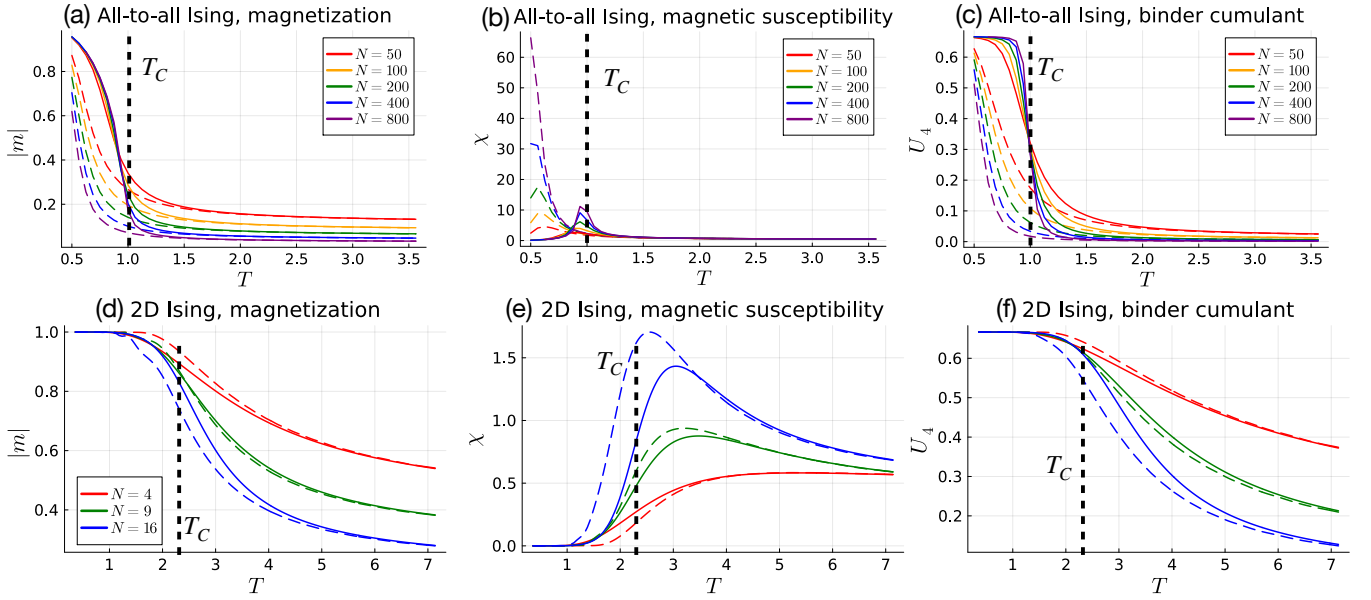


FIG. 3. Colored solid lines represent the theoretical values of the observables, their corresponding dashed lines represent the DQA-estimated values. The vertical black dashed lines represent the phase transition point. (a-c) The magnetizations, the magnetic susceptibilities and the binder cumulant of the all-to-all model. (d-f) The magnetizations, the magnetic susceptibilities and the binder cumulant of the 2D Ising model.

Let's consider the RBMs composed of n_v number of visible nodes and n_h number of hidden nodes. The two layers are fully connected, bipartitely. J_{ij} denotes the connection between i -th visible node and j -th hidden node. Also, the bias vectors defined on each layer will be represented by **a** and **b**. These correspond to z -directional external magnetic field of spin glass system. Then, the corresponding Hamiltonian is written by

$$\hat{H}_m = \sum_{1 \leq i \leq n_v} a_i \sigma_i^z + \sum_{1 \leq j \leq n_h} b_j \sigma_{n_v+j}^z + \sum_{1 \leq i \leq n_v, 1 \leq j \leq n_h} J_{ij} \sigma_i^z \sigma_{n_v+j}^z, \quad (12)$$

where i, j indicate site of nodes. a_i and b_j are the magnetic fields imposed on spins, while J_{ij} are interaction rate between two spins. The model's distribution is obtained from the Boltzmann distribution as

$$Q_V(\mathbf{s}_v) = \sum_{\mathbf{s}_h} Q_{VH}(\mathbf{s}_v, \mathbf{s}_h) = \sum_{\mathbf{s}_h} \frac{1}{Z} \langle \mathbf{s}_v \mathbf{s}_h | \exp(-\hat{H}_m) | \mathbf{s}_h \mathbf{s}_v \rangle, \quad (13)$$

where \mathbf{s}_v and \mathbf{s}_h are spin- z configurations of the visible and hidden nodes. The eigenstates of \hat{H}_m , $|\mathbf{s}_v \mathbf{s}_h\rangle$, are given by spin- z configurations and Z is the partition function, $Z = \text{tr}(\exp(-\hat{H}_m))$. One can notice that we represent the Hamiltonian using the Pauli matrix, σ^z , which allows us to describe the quantum dynamics of DQA.

When applying the gradient descent, the error to be decreased is the Kullback-Leibler divergence between the training data's distribution, $P_V(\mathbf{s}_v)$ and the model's dis-

tribution, $Q_V(\mathbf{s}_v)$, defined by

$$D_{\text{KL}}(P_V|Q_V) = \sum_{\mathbf{s}_v} P_V(\mathbf{s}_v) \ln \left(\frac{P_V(\mathbf{s}_v)}{Q_V(\mathbf{s}_v)} \right). \quad (14)$$

For one step of the gradient descent, the parameters at \hat{H}_m are updated by following the rule,

$$\begin{aligned} a_i(t+1) &= a_i(t) - \alpha \frac{\partial D_{\text{KL}}(P_V|Q_V)}{\partial a_i} \\ b_j(t+1) &= b_j(t) - \alpha \frac{\partial D_{\text{KL}}(P_V|Q_V)}{\partial b_j} \\ J_{ij}(t+1) &= J_{ij}(t) - \alpha \frac{\partial D_{\text{KL}}(P_V|Q_V)}{\partial J_{ij}}, \end{aligned} \quad (15)$$

for a learning rate α .

It was studied that the derivative of the Kullback-Leibler divergence is equal to the difference between expectation values from P_V and Q_V . Explicitly, the derivative is written as

$$\begin{aligned} \frac{\partial D_{\text{KL}}(P_V|Q_V)}{\partial a_i} &= \langle s_i \rangle_{Q_V} - \langle s_i \rangle_{P_V} \\ \frac{\partial D_{\text{KL}}(P_V|Q_V)}{\partial b_j} &= \langle s_j \rangle_{Q_{VH}} - \langle s_j \rangle_{Q_{H|V}P_V} \\ \frac{\partial D_{\text{KL}}(P_V|Q_V)}{\partial J_{ij}} &= \langle s_i s_j \rangle_{Q_{VH}} - \langle s_i s_j \rangle_{Q_{H|V}P_V}. \end{aligned} \quad (16)$$

$\langle s_i \rangle_P$ is expectation value of $\langle s_{v,i} | \sigma_i^z | s_{v,i} \rangle$ over the probability, P . Likewise, $\langle s_j \rangle$ is expectation value

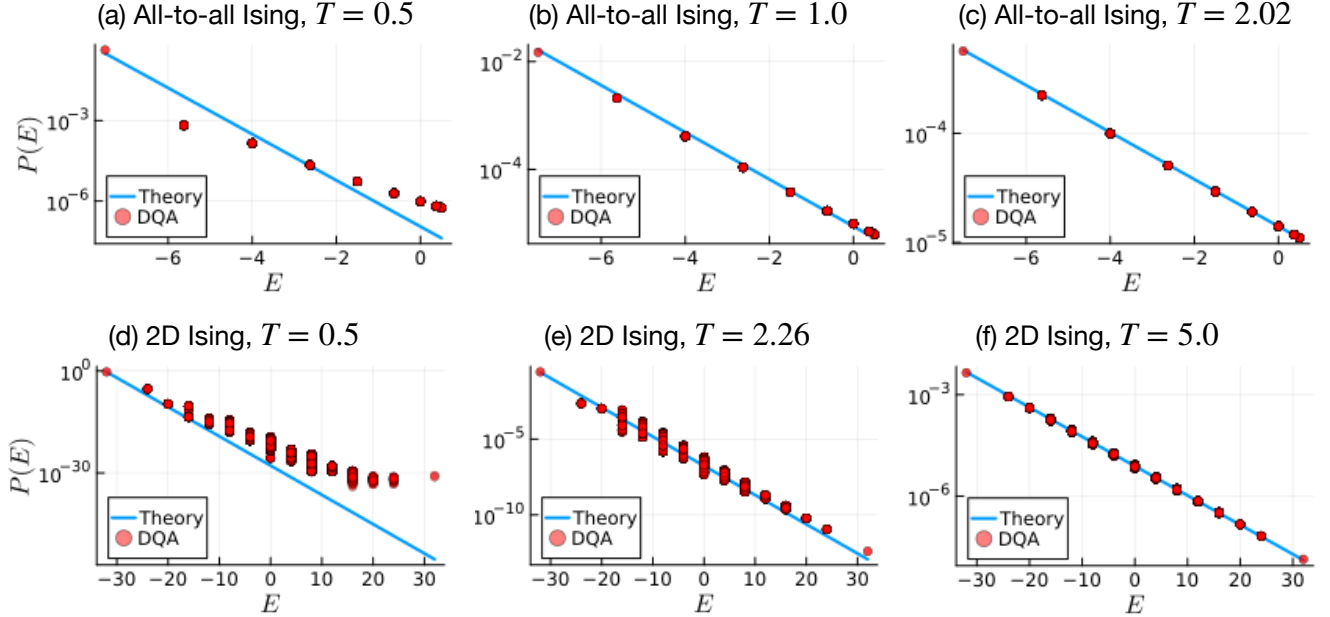


FIG. 4. Blue lines represent the theoretical Boltzmann distributions of the RBMs. The red dots represent the energies of all possible states of the RBMs estimated by the DQA. (a-c) The magnetizations, the magnetic susceptibilities and the binder cumulant of the all-to-all Ising model. (d-f) The magnetizations, the magnetic susceptibilities and the binder cumulant of the 2D Ising model. As the temperature of the system is lower, the quality of the distribution estimated by the DQA is lower.

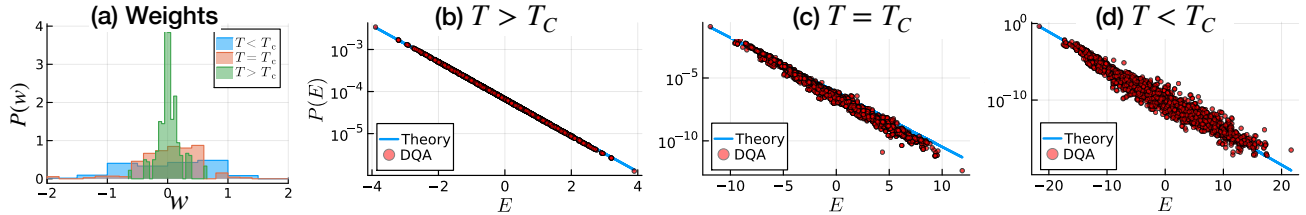


FIG. 5. (a) Weight distribution of RBMs reproducing 2-d Ising configurations at given temperatures. 10 trained matrices are used. The smaller the weight deviation, the better the DQA performance. (b-d) The Boltzmann distribution represented by the RBM (blue line) and its estimated distribution by DQA (black dots). These are the results from the RBMs trained by (b) disordered data ($T=16$ 2D Ising model) (c) critical data ($T=3.6$ 2D Ising model) (d) ordered data ($T=1.9$ 2D Ising model).

of $\langle s_{h,j} | \sigma_{n_v+j}^z | s_{h,j} \rangle$ and $\langle s_i s_j \rangle$ is expectation value of $\langle s_{v,i} s_{h,j} | \sigma_i^z \sigma_{n_v+j}^z | s_{v,i} s_{h,j} \rangle$. We mention that $Q_{H|V} P_V$ is usually not normalized, but the equation Eq. (16) holds when $Q_{H|V} P_V$ is dealt with as the positive measure.

In Sec. II, we introduced a new sampling scheme, DQA. By using the new method, the estimation of Boltzmann distribution represented by the RBMs will be possible. We did not use DQA for training RBMs, however, using the trained RBMs, we compared the probability distribution of the RBMs and estimated distribution using DQA in Fig. 5. This work corresponds to what happens during one epoch in real training.

The RBMs are trained results by using datasets from 2-dimensional Ising model of various temperatures. Fig. 5(a) shows the histogram of the weight components of each RBMs. When disordered data ($T > T_C$) are used,

the weight components are concentrated around 0. When ordered data ($T < T_C$) are used, the weight components are distributed between -1 to 1, relatively evenly. The critical temperature case ($T = T_C$) appears to be something in between the two cases. Fig. 5(b-d) show the comparison of the RBMs' Boltzmann distribution (blue lines) and the DQA's estimated distribution (red points). When the weight components are staying in small value regime, the accuracy of DQA can be evaluated as high. In the remaining cases, the trend of the target distribution is well followed, with spread occurring.

In general, the training dynamics of artificial neural networks commonly proceed with the application of regularizers to prevent the weights from growing excessively. This ensures that our proposed sampling method operates within a regime characterized by high accuracy.

Consequently, DQA is expected to demonstrate substantial practical utility.

So far, many other studies tried to utilize quantum annealing to train the RBMs [2–5]. However, the sampling result of adiabatic quantum annealing is supposed to be the Boltzmann sampling of $\beta = \infty$, which means, only ground state is the original target of the sampling process. Of course the hardware spec of D-wave corporation are not yet perfect, the sampling results contain a few excited states making the distribution closer to some low temperature Boltzmann distribution. However, it is closer to a coincidence rather than a logical conclusion.

V. DERIVATION DETAILS

Denoting by \mathbf{r} the z -directional spin configuration, the problem Hamiltonian \hat{H}_P can generally be written as

$$\hat{H}_P = \sum_{\mathbf{r}} E_{\mathbf{r}} |\mathbf{r}\rangle\langle\mathbf{r}|. \quad (17)$$

Meanwhile, we can also write $\hat{H}_P = \sum_n \hat{H}_{P,n}$, where

$$\hat{H}_{P,n} = - \sum_{i_1 < \dots < i_n} J_{i_1 \dots i_n} \sigma_{i_1}^z \dots \sigma_{i_n}^z \quad (18)$$

represents the n -spin interactions. Combining these two expressions, the energy of each \mathbf{r} can also be expressed as $E_{\mathbf{r}} = \sum_n \langle \mathbf{r} | \hat{H}_{P,n} | \mathbf{r} \rangle = \sum_n E_{\mathbf{r},n}$.

Treating \hat{H}_P as a perturbation, from now on we use its interaction-picture representation

$$\begin{aligned} \hat{H}_P(t) &= e^{-i \int_t^T d\tau A(\tau) \hat{H}_x} \hat{H}_P e^{i \int_t^T d\tau A(\tau) \hat{H}_x} \\ &= \sum_n e^{-i \int_t^T d\tau A(\tau) \hat{H}_x} \hat{H}_{P,n} e^{i \int_t^T d\tau A(\tau) \hat{H}_x} \\ &\equiv \sum_n \hat{H}_{P,n}(t). \end{aligned} \quad (19)$$

Then, using the Dyson series expansion of Eq. (3), the final state $|\psi_f\rangle$ reached after the annealing procedure can be expressed as

$$\begin{aligned} |\psi_f\rangle &= \left[1 - i \int_0^T dt B(t) \hat{H}_P(t) \right. \\ &\quad \left. + (-i)^2 \int_0^T dt_1 \int_0^{t_1} dt_2 B(t_1) \hat{H}_P(t_1) B(t_2) \hat{H}_P(t_2) + \dots \right] \\ &\quad \times e^{iN \int_0^T d\tau A(\tau)} \bigotimes_{i=1}^N |X-\rangle_i. \end{aligned} \quad (20)$$

For convenience, let us define $\phi_t \equiv \int_t^T d\tau A(\tau)$. Since \hat{H}_x rotates each Pauli operator by the same phase $2\phi_t$, we can rewrite $\hat{H}_{P,n}(t)$ as

$$\hat{H}_{P,n}(t) = - \sum_{i_1 < \dots < i_n} J_{i_1 \dots i_n} \sigma_{i_1}^z(t) \dots \sigma_{i_n}^z(t), \quad (21)$$

where $\sigma_i^z(t) \equiv \cos(2\phi_t) \sigma_i^z - \sin(2\phi_t) \sigma_i^y$.

Plugging Eq. (21) into Eq. (20) and using

$$\begin{aligned} \sigma_i^z(t) |X-\rangle_i &= [\cos(2\phi_t) \sigma_i^z - \sin(2\phi_t) \sigma_i^y] |X-\rangle_i \\ &= [\cos(2\phi_t) \sigma_i^z - i \sin(2\phi_t) \sigma_i^z] |X-\rangle_i \\ &= e^{-2i\phi_t} \sigma_i^z |X-\rangle_i, \end{aligned} \quad (22)$$

we obtain

$$\begin{aligned} |\psi_f\rangle &= e^{iN\phi_0} \left[1 - i \sum_n \int_0^T e^{-2ni\phi_t} B(t) \hat{H}_{P,n} \right. \\ &\quad \left. + \mathcal{O}(\hat{H}_{P,n}^2) \right] \bigotimes_{i=1}^N |X-\rangle_i, \end{aligned} \quad (23)$$

which yields the projective probability

$$\begin{aligned} P_Q(\mathbf{r}) &= |\langle \mathbf{r} | \psi_f \rangle|^2 \\ &= \frac{1}{2^N} \left[1 - 2 \sum_n E_{\mathbf{r},n} \int_0^T dt B(t) \sin(2n\phi_t) + \mathcal{O}(E_{\mathbf{r},n}^2) \right]. \end{aligned} \quad (24)$$

We require that, up to order $E_{\mathbf{r},n}$, this projective probability should be equal to the Boltzmann distribution

$$P_B(\mathbf{r}) = \frac{1}{Z'} e^{-\beta E'_{\mathbf{r}}} = \frac{1}{2^N} \left[1 - \beta E'_{\mathbf{r}} + \mathcal{O}(\beta^2 E'^2_{\mathbf{r}}) \right], \quad (25)$$

of modified Hamiltonian $\hat{H}' = \sum_n c_n \hat{H}_{P,n}$ by first order of $E'_{\mathbf{r}} = \sum_n c_n E_{\mathbf{r},n}$, where β is given by

$$\beta = 2 \int_0^T dt B(t) \sin \left(2 \int_t^T ds A(s) \right), \quad (26)$$

and the modifying factor c_n is given by

$$c_n = \frac{\int_0^T dt B(t) \sin \left(2n \int_t^T ds A(s) \right)}{\int_0^T dt B(t) \sin \left(2 \int_t^T ds A(s) \right)}. \quad (27)$$

We provided a linear function of $A(t) = \alpha(T-t)$ with $B(t) = 1$ as the candidate of the schedule for the low-temperature Boltzmann sampling. Eq. (26) gives β as

$$\beta = 2 \int_0^\infty dt \sin(\alpha t^2) = \sqrt{\frac{\pi}{2\alpha}}, \quad (28)$$

while the modifying factor c_n is

$$c_n = \frac{\int_0^\infty dt \sin(\alpha nt^2)}{\int_0^\infty dt \sin(\alpha t^2)} = \frac{1}{\sqrt{n}}, \quad (29)$$

when T goes to infinity to satisfy the boundary condition, $A(0) = \alpha T \gg 1 = B(0)$.

VI. CONCLUSION

In this study, we took a closer look at quantum annealing again. By modifying the schedule from adiabatic

to diabatic linear process, namely diabatic quantum annealing, we showed analytically and numerically that the annealing speed is related to the specific temperature.

We firstly check the Kullback-Leibler divergences between theoretical distributions and the DQA-estimated ones are very small for high temperature regime. And as the system size increases, $D_{KL}(P_{\text{theory}} \| P_{\text{DQA}})$ lines collapse see Fig. 1 (b). It implies that the error rate is negligible for very large system.

Next, we check how much different the estimated probabilistic distributions obtained by DQA process and the target theoretical distributions of the artificial neural networks. For various kinds of featured data sets, the DQA-estimated distributions are close to the Boltzmann distribution of the model. The deviation of the components of weight matrix is the key that determines the quality of DQA. As the deviations is smaller, the similarity between DQA estimated and the theoretical distribution are high.

To summarize, effective temperature of the system is

the key that determines the quality of the DQA. Particularly, when a artificial neural network system is in lazy learning regime [15], the sizes of the weight matrix would be small and hardly changes, the DQA's estimation will be a good alternative to the conventional learning algorithm. Another case that the DQA would work well is when the system has very strong regularization condition.

All we have checked are linear schedule based DQA. We leave the exploration of various general schedules as future work.

ACKNOWLEDGMENTS

This work was supported by the Global-LAMP Program of the National Research Foundation of Korea (NRF) grant funded by the Ministry of Education (No. RS-2023-00301976).

[1] J. Preskill, Quantum Computing in the NISQ era and beyond, *Quantum* **2**, 79 (2018).

[2] V. Dixit, R. Selvarajan, T. Aldwairi, Y. Kosha, M. A. Novotny, T. S. Humble, M. A. Alam, and S. Kais, Training a quantum annealing based restricted boltzmann machine on cybersecurity data, *IEEE Transactions on Emerging Topics in Computational Intelligence* **6**, 417 (2022).

[3] L. Moro and E. Prati, Anomaly detection speed-up by quantum restricted boltzmann machines, *Communications Physics* **6**, 269 (2023).

[4] C. F. Higham and A. Bedford, Quantum deep learning by sampling neural nets with a quantum annealer, *Scientific reports* **13**, 3939 (2023).

[5] T. Pochart, P. Jacquot, and J. Mikael, On the challenges of using d-wave computers to sample boltzmann random variables, in *2022 IEEE 19th international conference on software architecture companion (ICSA-C)* (IEEE, 2022) pp. 137–140.

[6] T. Kato, On the adiabatic theorem of quantum mechanics, *Journal of the Physical Society of Japan* **5**, 435 (1950).

[7] T. Kadowaki and H. Nishimori, Quantum annealing in the transverse ising model, *Phys. Rev. E* **58**, 5355 (1998).

[8] J. Raymond, S. Yarkoni, and E. Andriyash, Global warming: Temperature estimation in annealers, *Frontiers in ICT* **3**, 10.3389/fict.2016.00023 (2016).

[9] R. Sandt and R. Spatschek, Efficient low temperature monte carlo sampling using quantum annealing, *Scientific Reports* **13**, 6754 (2023).

[10] <https://www.dwavesys.com> () .

[11] Performance advantage in quantum boltzmann sampling () .

[12] G. E. Hinton, Training products of experts by minimizing contrastive divergence, *Neural Computation* **14**, 1771 (2002).

[13] D. J. Earl and M. W. Deem, Parallel tempering: Theory, applications, and new perspectives, *Physical Chemistry Chemical Physics* **7**, 3910 (2005).

[14] D. H. Ackley, G. E. Hinton, and T. J. Sejnowski, A learning algorithm for boltzmann machines, *Cognitive science* **9**, 147 (1985).

[15] M. Geiger, S. Spigler, A. Jacot, and M. Wyart, Disentangling feature and lazy training in deep neural networks, *Journal of Statistical Mechanics: Theory and Experiment* **2020**, 113301 (2020).